Journal of Volcanology and Geothermal Research 237-238 (2012) 97–111

Contents lists available at SciVerse ScienceDirect

Journal of Volcanology and Geothermal Research

journal homepage: www.elsevier.com/locate/jvolgeores

Geological relationships of basalts, andesites and sand injectites at the base of the Paraná volcanic province, Torres, Brazil

L.A. Hartmann *, K.R. Arena, S.K. Duarte

Instituto de Geociências, Universidade Federal do Rio Grande do Sul, Avenida Bento Gonçalves, 9500, 91501-970 Porto Alegre, Rio Grande do Sul, Brazil

ARTICLE INFO

Article history:
Received 7 December 2011
Accepted 24 May 2012
Available online 2 June 2012

Keywords:
Paraná volcanic province
Torres
Sand injectites
Intrusive breccias
Lava stratigraphy
Lava correlation

ABSTRACT

The Cretaceous interaction of the heated, giant Guarani aquifer with lavas, dikes and sills of the Paraná volcanic province is here evaluated based on the description of the large exposures in Torres, southernmost Brazil. Chalcedony silicified sandstone dikes, sills and breccias containing volcanic clasts in a sandstone matrix are common in the Paraná volcanic province. Sandstone layers mark either the contact between lava flows or the base of the vertically-jointed, massive core. In Torres, one basaltic andesite and one andesite lava flow of the low-Ti Gramado type, and basalt and basaltic andesite sills and dikes, are correlated over 10 km with rocks in the Graxaim quarry. Scintillometric emission rates vary systematically with contents of K, Th and U and are characteristic of each lava or intrusive rock. Major and trace elements are also characteristic of each lava. Three large outcrops of breccias display angular, amygdaloidal volcanic clasts immersed in a silicified sandstone matrix. No evidence was found of high temperature (1150 °C) interaction of the lava with the loose, erg of the Botucatu Formation, such as fluidal volcanic clasts, quenched rims or thermal recrystallization of the sand; only a thin (5 mm) layer of thermally modified sand is present on top of a paleodune in Torres.

In Torres, the interaction of andesite with wet sand occurred after degassing of the lava, because the breccia clasts are amygdaloidal. All evidence points to hydrothermal processes for the formation of the breccias, such as lozenge fractures filled with silicified sandstone, preserved detrital characteristics of the sandstone grains and cold (below 130 °C) contact between the volcanic rock and the sand. Most significant is the timing of sand intrusion, because thin (1 mm) dikes of silicified sandstone cut fractures in the rock and the zeolite-filled amygdales. The sandstone dikes, sills and breccias are interpreted as a result of the ascent of overpressured heated water and its vapor from the huge, underlying Guarani aquifer, carrying fluidized sand and continuously silicifying the intruded sand. The three breccias are sills intruded into cold lava flows. The description and correlation of the magmatic bodies and the field relationships of the silicified sandstones establish the stratigraphy of the Paraná volcanic province in Torres and elucidate the processes responsible for the injection and effusion of sand in the Cretaceous.

1. Introduction

The Paraná volcanic province is a giant, bimodal basalt–rhyodacite sequence that comprises the Serra Geral Group located in southeastern South America. The province evolution poses major questions that require investigation, including the sequence and correlation of magmas generated in the beginning of magmatism and the interaction of a large number of small-volume sand injectites and extrudites (nomenclature of Hurst et al., 2011) along the entire volcanic stratigraphy. Magmatic processes are not evaluated here; they are related to variable extents of melting of lithospheric and asthenospheric mantle, followed by crustal contamination and magma fractionation (e.g., Hartmann et al., 2010a and references therein).

The discovery of the geological controls for sand mobilization and injection in volcanic rocks (Hartmann et al., 2012) in the Cretaceous Paraná volcanic province (~135 Ma; Pinto et al., 2011a; Janasi et al., 2011) of South America indicates that water and its vapor from the huge Guarani aquifer attained 130 °C during lozenge fracturing of the lava flows and sand fluidization with accompanying hydrothermal breccia intrusion. Sand dikes are common in this volcanic province and in the underlying sedimentary Paraná basin (e.g., Arioli et al., 2008; Perinotto et al., 2008; Machado et al., 2009).

Comparable continental flood basalt provinces in the world are underlain by weak aquifers and only display minor sand mobilization, e.g., Columbia River (USA), Karoo (South Africa) and Deccan (India). The Paraná volcanic province offers a unique opportunity to study the tectonic and hydrothermal interaction of two large geological structures, the Guarani aquifer and the Serra Geral Group of basalts and rhyodacites.

* Corresponding author. Tel.: +55 51 33087202; fax: +55 51 33087203.
E-mail address: leo.hartmann@ufrgs.br (L.A. Hartmann).

0377-0273/$ – see front matter © 2012 Elsevier B.V. All rights reserved.
doi:10.1016/j.jvolgeores.2012.05.017

The dynamic interaction of loose sand with overlying seal layers is a common process in offshore petroleum basins, resulting in the injection of large volumes of fluidized sand as dikes and sills into the overlying claystones and extrudites at the sea bottom (e.g., Huuse et al., 2010; Vétel and Cartwright, 2010; Hurst et al., 2011). It is also a significant process in continental basins where sand is mobilized by water. For instance, large-scale erg sand injection into overlying Jurassic units in Idaho included the ascent of meter-sized clasts of sedimentary rocks (Huuse et al., 2005). The entire set of sand bodies can be designated "sand injectites" and includes sand dikes, sills, lopoliths, cups, volcanoes, flows and breccias (Hurst et al., 2011).

The fluid in the offshore basins is commonly at 20–70 °C and the injected sand bodies remain highly porous; e.g., Schwab et al. (2011) observed that "the injected sands are an excellent reservoir with consistently high porosity and permeability" in offshore Norway basins. A mudstone is the most common caprock because this abundant rock type constitutes the impermeable seal that is required for the development of overpressure in the fluid (commonly water or oil).

In the Paraná volcanic province, sand dikes, sills and breccias are common features over the entire extent of the province and along most of the stratigraphic column of the Serra Geral Group (1800 m at depocenter, 300 km to the northwest of the studied area), which has ~120 lava flows (e.g., Pinto and Hartmann, 2011; Pinto et al., 2011b; Hartmann et al., 2012). In the central region of the province, Waichel et al. (2007) registered the occurrence of numerous breccias containing basalt clasts in a sandstone matrix and considered the rocks as peperites formed by the interaction of hot lava with wet sand. In the presently studied region, sand dikes were described by Petry et al. (2007), whereas Arioli et al. (2008) described numerous sand dikes and layers in the state of Paraná, located 600 km to the northwest of Torres. The breccias in the Torres hills were considered by Petry et al. (2007) as dry peperites. It is also novel that the caprocks for sand intrusion in this continental province are basalt lava flows (also andesite, rhyodacite) and not mudstones as in offshore basins (e.g., Schwab et al., 2011) and in most environments that display sand intrusion. It is also significant that the sand bodies in the Paraná volcanic province are intensely silicified and have very low porosity, in strong contrast with the sand injection complexes of offshore petroleum basins.

Numerous sandstone dikes, sills and breccias are well-exposed at the sea cliffs of Torres, Brazil (Petry et al., 2007), intrusive into lava flows of the Serra Geral Group (Fig. 1).

We propose a model of sand injection by low-temperature hydrothermal processes into basaltic rocks from Torres, opposed to a previous hypothesis (Petry et al., 2007) that proposed high-temperature lava–sediment interaction for the same outcrops. Field observations are the basis of this novel hypothesis, supported by gamma-ray scintillometry and geochemical analyses of rocks. We also establish the stratigraphy and correlation of lava flows, sills and dikes in this basal portion of the Paraná volcanic province.

This is a case-study in Torres of the general process registered over the entire ~1,000,000 km^2 area covered by the volcanic sequence of the Serra Geral Group in Brazil, Paraguay, Argentina and Uruguay.

2. Methodology

The observation of satellite images was followed by field trips to the Torres region, particularly the sea cliff exposures in the hills. The Graxaim quarry is named after a local mamifer resembling a fox, and was also studied due to the relationship of sandstone dikes with zeolite-filled amygdales and their association with the two lava flows present. The quarry is situated ~300 m from the BR-101 highway, 10 km southwest of the Cabras hill in Torres (Fig. 2a). The Torres hills and Graxaim quarry are here designated "Torres region".

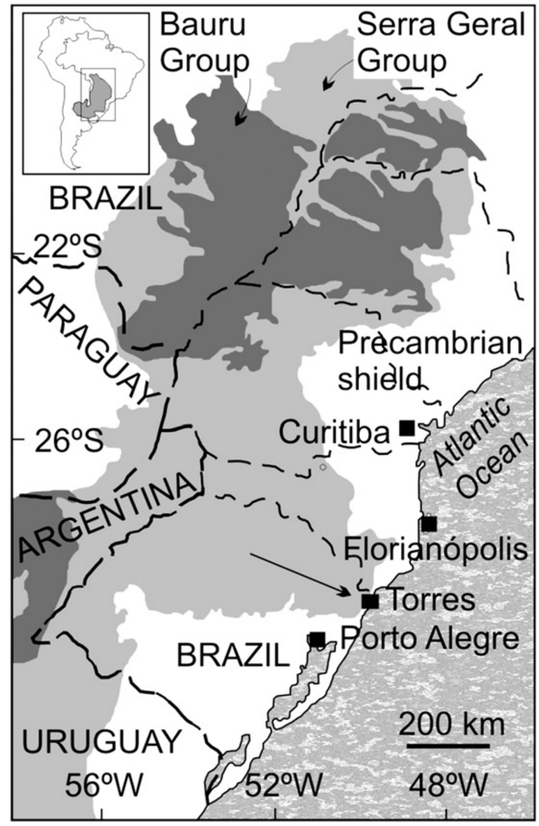

Fig. 1. Geological map displaying the area of occurrence of the Serra Geral Group and sedimentary cover of Paraná basin (Peate et al., 1992). The Torres town, where the studied region is located, is indicated by an arrow.

The detailed study of the exposures during field work was integrated with scintillometric (gamma-spectrometric) measurements and rock geochemistry to reach a better understanding of the unique relationships of hot water and its vapor with loose, desert dune sand buried by volcanic caprocks. A portable gamma ray scintillometer model GR0110G, by SAIC Exploranium, was used for the emission rates measurements. Measurements (n = 10–15, cps = counts per second) were registered in all visited outcrops. This is the total gamma-ray rate of emission from radioactive elements, mostly K, U and Th.

Selected rock samples from the four studied hills and from the Graxaim quarry were analyzed for major and trace elements in the ACME laboratory, Canada, using analytical procedures named by ACME as "Group 4A and Group 4B". Group 4A analyses used $LiBO_2$ fusion/dilute nitric digestion then ICP-ES for major oxides plus minor elements; LOI is weight loss on ignition. Group 4B analyses of rare earths and refractory elements used ICP-MS. All data were integrated and interpreted with the support of computers at Universidade Federal do Rio Grande do Sul, using Excel and GCDKit software. Because the major element composition of the rocks was strongly modified by hydrothermal processes, we used a mixed classification of major and less-mobile trace elements to classify the rocks. The geochemical alteration is indicated by positive or negative correlation of the oxide (or element) with LOI. A major elements (e.g., TAS) diagram was used for a general evaluation of rock classification in low-LOI (less than 2.0 wt.%) analyses, but emphasis was placed on the Nb/Y versus Zr/TiO_2 diagram.

3. Geological relationships

The Paraná volcanic province (e.g., Peate et al., 1992; Hartmann et al., 2010a,b) in South America (Fig. 1) is near the top of the

Fig. 2. Satellite images of studied region. (a) Graxaim quarry and studied hills in Torres town = Farol, Furnas, Guarita, Cabras hills; (b), (c) and (d) Location of geological sections A and B (Fig. 3) and of analyzed samples. Codes for samples: 1 = T1A; 2 = T1B; 3 = T3; 4 = T2A; 5 = T2B, T2C; 6 = T4A; 7 = T4B, B1A, B1B, B1C; 8 = T4C; 9 = T4D, B2A, B2B, B2C; 10 = T4E, T4E1; 11 = T4F, T4F1; 12 = T5A, T5A1; 13 = T5B, T5B1, T5B2; 14 = T5C, T5C1; 15 = T1C; 16 = T5D, T5 E, T5F.

7000 m Paraná basin, only partly covered by the Bauru Group of sedimentary rocks (Zalán et al., 1991) and has mostly basalts, basaltic andesites, andesites, rhyodacites and dacites included in the Serra Geral Group. Some remarkable features are present in the exposures of volcanic rocks in the Torres region (Figs. 2, 3, 4, 5, 6, 7, 8, 9) and deserve description, including the fault structure of the volcanic rocks, the presence of the underlying Botucatu Formation sandstone at the beach level, the sandstone–andesite breccias, the silicified sandstone layer on top of a breccia, the dikes and sills of silicified sandstone, the presence of silicified sandstone in lozenge fractures

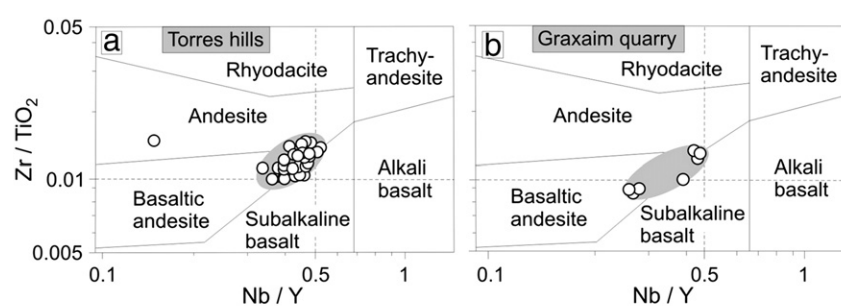

Fig. 3. Chemical classification of volcanic rocks from Torres and Graxaim quarry showing predominance of basaltic andesites, but basalt and andesite also present.

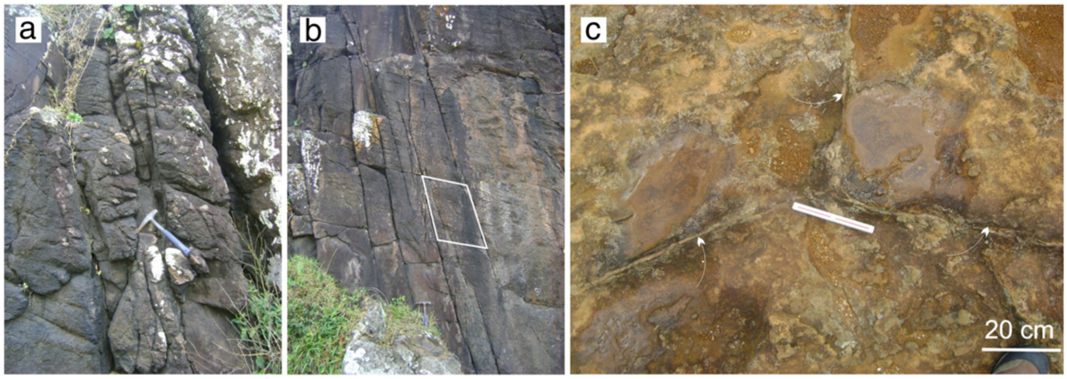

Fig. 4. Field photos of Viola sill in the Cabras hill. (a) Subvertical, brittle fault zone that cuts the older lozenge fractures; (b) lozenge fractures; (c) plan view of silicified sandstone dikes in fractures of andesite, at the top of Cabras hill, indicated by three white arrows.

of the andesite, the crosscutting relationship of thin sandstone dikes with zeolite-filled amygdales, and the presence of 10–20 cm-size quartz geodes. All these features are here described and require an integrated model for the understanding of the geological evolution of the region in the Cretaceous.

3.1. Geology of Torres hills

Four extensive outcrops were described in four hills in Torres town (Fig. 2a, b, c and d). The hills rise up to 50 m above sea level and are directly hit by normal and storm waves, resulting in large, fresh rock exposures. Humid climate (cold winter — 0–10 °C, hot summer — 25–35 °C) resulted in thick soil with grass and shrub cover with few rock exposures, except at the cliffs. Some of the main features of the geological units are presented in Table 1.

Two lava flows were recognized from field relationships, geochemistry and scintillometry. The rocks were initially classified based on major element compositions of samples with the lowest loss on ignition, but the strong hydrothermal alteration prohibits the procedure. Trace element compositions of less-mobile elements are used and are close to the limits between subalkaline basalt, basaltic andesite and andesite (Fig. 3).

The Cabras hill is made up of massive, fine to medium-grained andesite. No lower or upper amygdaloidal crusts are exposed; the lower contact is below sea level and the top of the hill displays cross-sections of columnar joints indicating erosion of the upper contact. Several subvertical, brittle fault zones cut the hill (Fig. 4a), and are part of the large-scale transcurrent fault system that is present along the eastern border of the Paraná basin (Jacques et al., 2010). Many vertical fractures form 0.5–2.0 m size blocks; these are reminiscent of cooling joints, particularly in the upper part of the hill, but the integrated set of vertical and inclined fractures results in lozenge-shaped blocks in the lower and middle portion of the hill (Fig. 4b). The inclined fractures cut across the contacts of the subvertical blocks, so they are not cooling structures of the lava. On top of the Cabras hill, many thin (0.1–1.0 mm) nearly vertical, dikes and some thin (0.1–1.0 mm) sills of silicified sandstone are present. Only at the top of the hill are silicified sandstone dikes observed that intrude fractures (Fig. 3c). Neither breccia nor Botucatu Formation sandstone is present at the base of this hill.

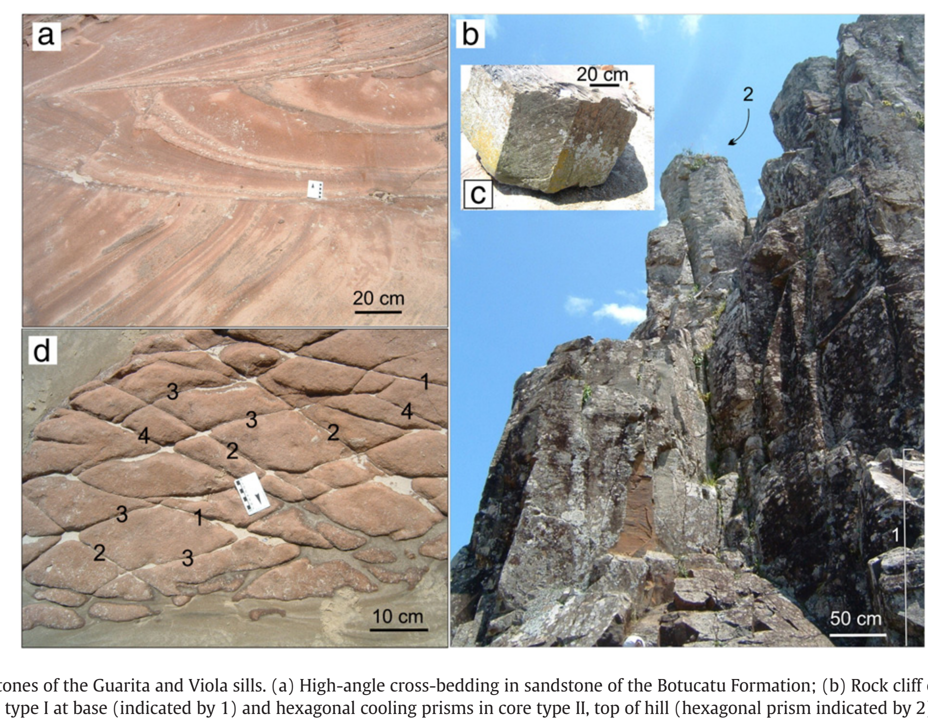

Fig. 5. Field photos of sandstones of the Guarita and Viola sills. (a) High-angle cross-bedding in sandstone of the Botucatu Formation; (b) Rock cliff of Guarita hill, displaying massive, lozenge-fractured, core type I at base (indicated by 1) and hexagonal cooling prisms in core type II, top of hill (hexagonal prism indicated by 2); (c) fallen block of hexagonal prism; (d) lozenge fractures (four families) in the upper surface of a silicified sandstone layer (20 cm thick).

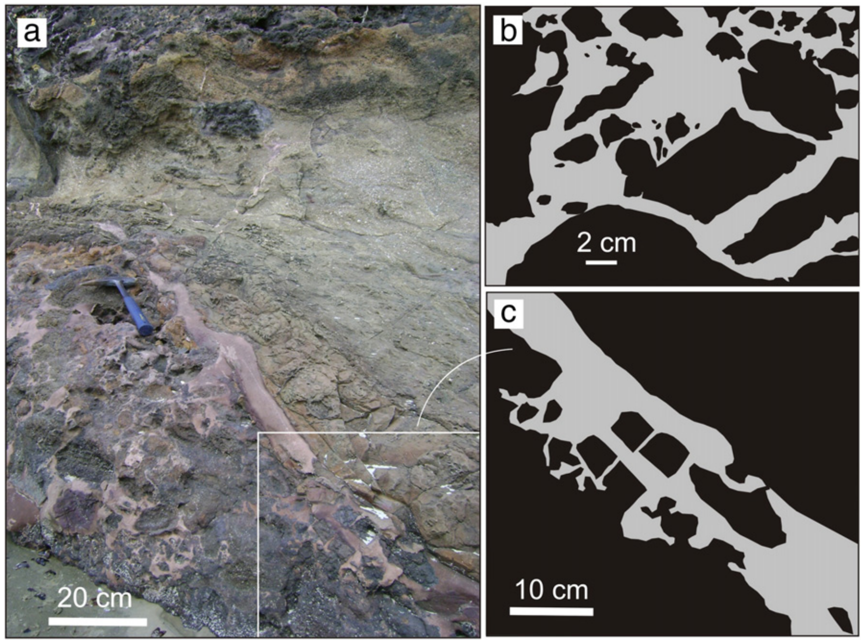

Fig. 6. Breccia 1 at the southern base of Furnas hill. (a) Amygdaloidal crust disrupted by brecciation; (b) and (c) sketch of angular shape of andesite clasts in this outcrop.

A smaller andesite remnant (Guarita hill) overlies a cross-bedded, poorly cemented, multiple-set sandstone of the Botucatu Formation (Fig. 5a). The andesite is fine- to medium-grained, massive, with no visible lower or upper amygdaloidal crusts. In the upper portion of the volcanic exposure (Fig. 4b, c), vertical, approximately hexagonal, columns are well-developed, similar to structures formed during lava cooling. This is considered a sill because no evidence was encountered of lava flow structures, such as lower or upper crust or horizontal jointing near the base.

No structural evidence of subaerial effusion of lava was observed in the Cabras and Guarita hills, such as upper and lower amygdaloidal crusts or horizontal jointing at the base or top of the igneous unit. The Guarita hill has a lower core type I without columnar jointing displaying lozenge fractures and an upper core type II with columnar jointing. Silicified sandstone was only observed in one thin dike in this outcrop. There is no amygdaloidal crust or horizontal jointing present in the basal portion of the Guarita hill near the contact with the Botucatu Formation sandstone.

The 500 × 1000 m Furnas hill has more varied geological features. From south to north, along a cross section from the beach to the top of the hill, a 20-cm thick layer of medium silicification sandstone, displaying lozenge fractures at the surface (Fig. 5d) is at the beach level. Only horizontal layering is present in this sandstone, contrasting with the cross-bedding of the nearby Botucatu Formation (Fig. 5a). A remarkable 50 m long, 5 m thick, andesite–sandstone breccia overlies the sandstone. This breccia, named breccia 1 (Fig. 6a), is made up of angular clasts (5–50 cm) of amygdaloidal andesite in medium silicified sandstone matrix. The breccia is usually clast-supported, with a few matrix-supported portions and is intrusive into the amygdaloidal crust of the flow. Jig-saw structures are common in the breccia which has mostly angular blocks (Fig. 6b, c). The main characteristics of the breccia are presented in Table 2.

An outstanding feature of the Furnas hill section is the presence of a thick, irregular, ~10 m thick, andesite–sandstone breccia between the lower core type I (no vertical cooling joints) and upper core type II (with vertical cooling joints) of the andesite flow (Fig. 7a, b, c). Below the core type I, flat lying lozenge fractures are present and more inclined lozenge fractures occur higher up (Fig. 8a, b, c). It is followed by a massive andesite with quartz geodes and sand dikes; lozenge fractures are present and many of them are filled with silicified sandstone dikes (Fig. 8b). A one-meter thick irregular layer of amygdaloidal rock is present inside the lower core. At the top of the hill, the erosional remnant of a massive volcanic unit is present and poorly exposed, and only massive rock was observed.

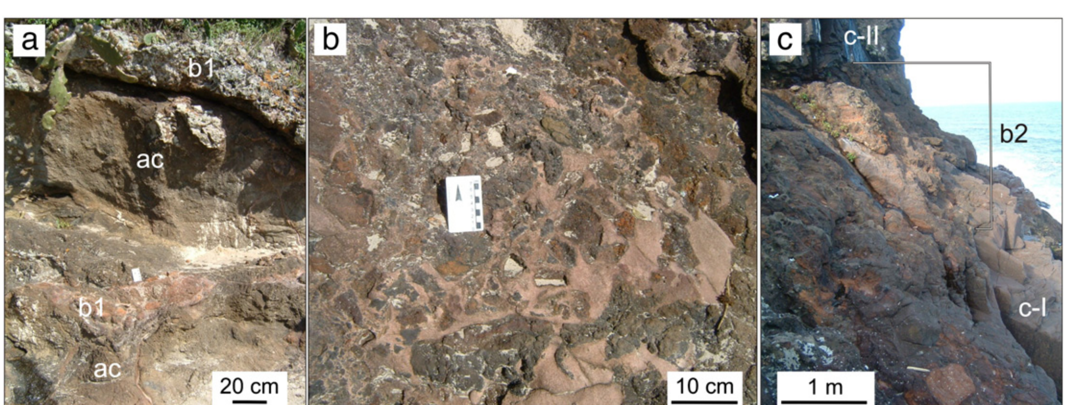

Fig. 7. Field photos of breccias 1 and 2 from the Furnas hill. (a) Breccia 1 (indicated as b1), containing andesite clasts and disrupted amygdaloidal crust (ac) of andesite; (b) angular shapes of andesite clasts of breccia 1; (c) position of breccia 2 (indicated as b2) between cores type I (c-I) and type II (c-II) of Arraia flow (andesite).

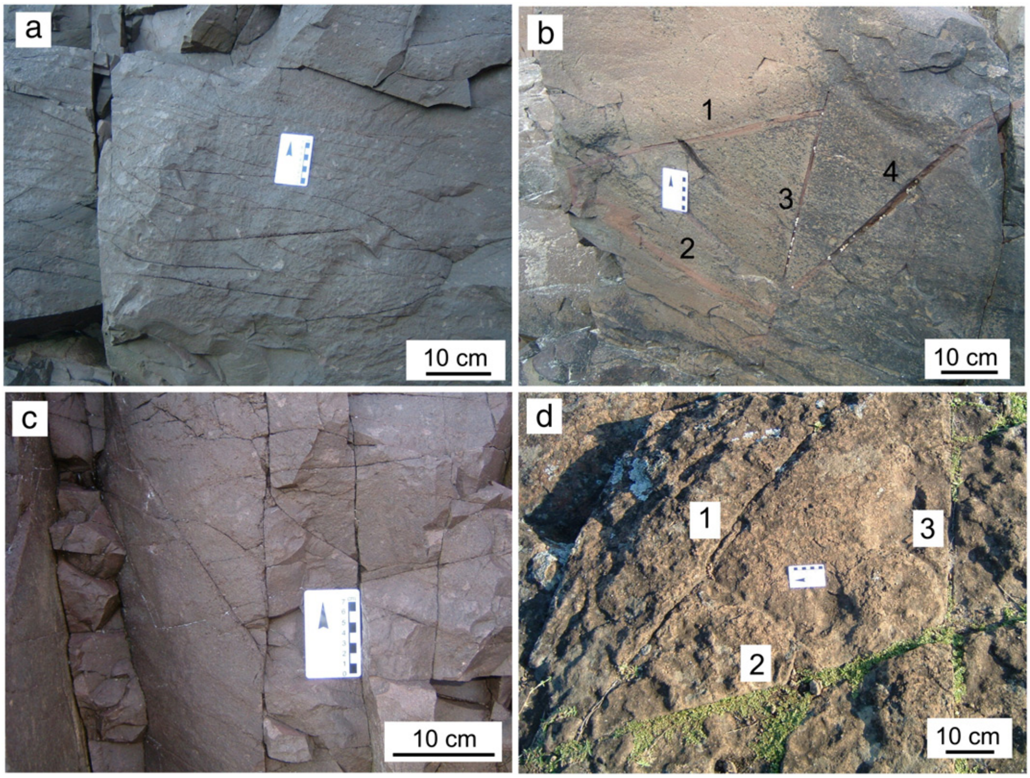

Fig. 8. Field photos of lozenge fractures in Arraia flow (andesite). (a) Lower portion of the type I core, close to contact with underlying breccia 1; (b) vertical face in middle portion of type I core, displaying four silicified sandstone dikes in lozenge fractures of andesite; (c) lozenge fractures in upper portion of core type I; (d) plan view of three lozenge fractures in the upper exposed surface of type II core. Some of the fractures contain silicified sandstone dikes.

The Farol hill is 100 × 500 m in area. A 100 × 50 m fresh outcrop of sandstone–basaltic andesite breccia 3 occurs in the Gruta da Santinha, near sea level (Table 2; Fig. 9a, b, c, d). The breccia has lava crust below and in lateral contact and is made up of fragments of basaltic andesite (10–50 cm large) in moderately silicified sandstone matrix. At the base of the cliff, the breccia evolves upward into massive sandstone containing a few, large (50 cm) angular clasts of basaltic andesite and then passing into a massive sandstone without clasts; a few uppermost, large (30 cm) clasts are immersed in sandstone.

Two basalt sills and one dike of similar composition (51.5 wt.% SiO_2) are exposed in the Gruta da Santinha (Farol hill), here designated the Gruta sills and dike. At sea level, a sill is exposed and continues underwater, intruded into the amygdaloidal basaltic andesite of the Santinha flow. A 10 cm thick basalt dike intrudes the amygdaloidal crust. At the vertical rock cliff of Gruta da Santinha, a sharp contact is present between a basalt sill (2-m thick, vertical jointing) and the thick, massive basaltic andesite with columnar jointing (core type II).

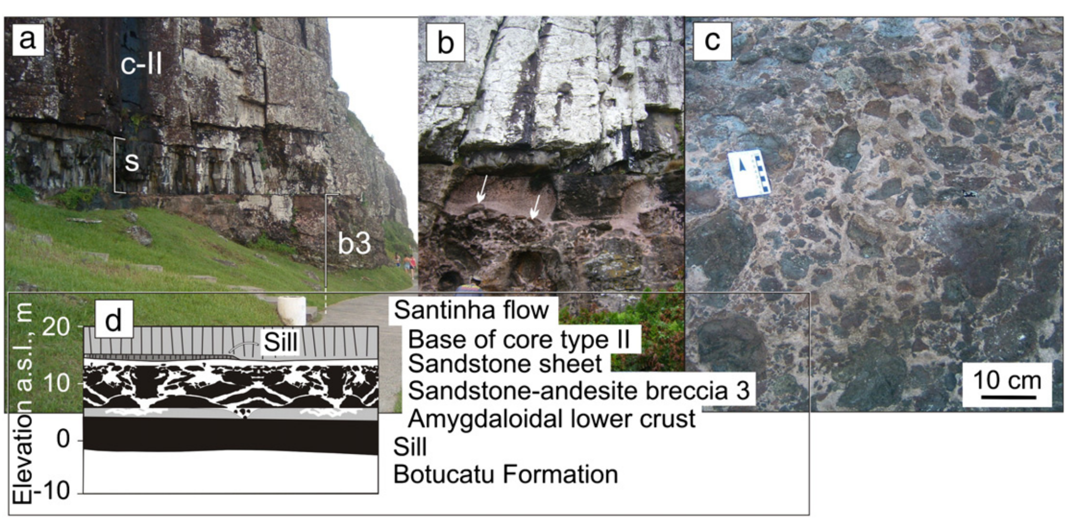

Fig. 9. Field photos and geological sketch of Santinha flow, Farol hill. (a) Breccia 3 (indicated as b3) showing sharp upper contact with basaltic sill (indicated as s) intruded into the Santinha flow core type II (indicated as c-II); (b) silicified sandstone sheet at the base of type II core, with up to 30 cm-large angular basaltic andesite clasts in the upper part; (c) angular basaltic andesite clasts in sandstone-supported breccia 3 at the beach level; (d) sketch of geological relationships of breccia 3.

Table 1
Selected characteristics of the Cretaceous geological units from Torres hills and Graxaim quarry. (–) = not applicable; (Est.) = estimated; Fm. = Formation; amygd. = amygdaloidal; cps values where available. “Breccia present” only refers to magmatic bodies. SiO_2 and TiO_2 cannot be estimated in Breccia 3 because of extreme modification of composition by hydrothermal processes. Only an estimative of SiO_2 composition of the analyzed rocks can be made because of strong hydrothermal alteration. “Sandstone dike, sill” were not analyzed chemically; it is a sill that turns into a dike along its length.

Unit number, name (cps)	Rock classification	Internal structure	Est. SiO_2 (wt.%)	TiO_2 (wt.%)	Sandstone dike, sill	Breccia present
Breccia 3, 90	Sandstone matrix	Mostly clast supported	–	–	Yes	–
	Basaltic andesite clast		52	1.20	Yes	
Breccias 1 and 2, 90	Sandstone matrix andesite clast	Mostly clast supported	54	1.75	Yes	–
Sand dike, sill	Silicified sandstone	Horizontal layering, silicified	–	–	–	–
Viola sill, 120	Andesite	Massive, no crust	57	1.56	Yes	No
Sill 2 + dike	Basaltic andesite	Massive, jointed	52.3	1.47	No	No
Gruta sills and dikes	Basalt	Massive, columnar joints	51.5	1.44	No	No
Arraia flow, 130	Andesite	Crusts poorly developed, core with lozenge fractures	60	1.39	Yes	Yes, at base
Santinha flow, 110	Basaltic andesite	Lower crust, core type II	54	1.30	Yes	Inside lower amygd. crust
Botucatu Fm., 100	Sandstone	High-angle cross-bedding	85	0.10	–	No

Table 2
Main characteristics of breccias from the Torres hills. Breccia 1 from the base of the southern cliff of the Furnas hill; breccia 2 from the middle of the cliff, Furnas hill; breccia 3 from Gruta da Santinha, Farol hill.

Location	Size of exposure	Position in flow	Structure	Sandstone	Matrix	Clast size (m)	Clast rock type	Clast shape
Breccia 1	30 m long, 2–5 m thick	Amygdaloidal crust	Mostly clast supported	At the base	Silicified sandstone	0.1–2.0	Andesite	Angular
Breccia 2	~15 m long, 1–5 m thick	Internal, center of core type I	Mostly clast supported	No	Silicified sandstone	0.1–1.0	Andesite	Angular
Breccia 3	50 m long, 3–10 m thick	Lower amygdaloidal crust, below core type II	Either matrix or clast supported	0.5–2.0 m thick, massive at the top, silicified	Silicified sandstone	0.1–0.8	Basaltic andesite	Angular

3.2. Geology of Graxaim quarry

The large (200×200 m in plan, 60 m high) Graxaim quarry has one basaltic andesite and one andesite flow and two sills (basalt and basaltic andesite), in addition to disrupted sandstone layers (Fig. 10; Table 1). Overall outcrop structure is made up of basaltic dikes and sills. The oldest unit is a restricted and intensely disrupted amygdaloidal crust, probably composing the upper crust of an underlying basaltic andesite flow. It is overlain by an andesite flow with massive core, upper and lower crusts, and containing poorly cohesive sandstone layers up to 1 m thick and 10 m long. Vertical, hexagonal cooling columns are common in the core. A 30 m thick basalt sill displays apophyses intrusive into the overlying sandstone. Thin (1–10 mm) silicified sandstone dikes cut the andesite flows but do not penetrate the basaltic sill. A younger basaltic andesite intrusion formed a composite sill and dike. Late brittle faults contain thin (~1 mm) veneers of calcite. No lozenge fractures or blocks were observed in the quarry. Hexagonal cooling columns are common in the sills.

Field relationships in the Torres region indicate therefore contacts of the lava flows, dikes and sills with sandstones of the Botucatu Formation. The main structures in the volcanic rocks are either related to cooling of the lava such as amygdaloidal crusts and core type II with hexagonal cooling joints or to tectonic processes acting on solid rock resulting in faults and fractures, some of them with lozenge shapes. The position of the breccias in the lower crust and in the core of lava flows, along with sandstone dikes and sills, requires an integrated, consistent explanation.

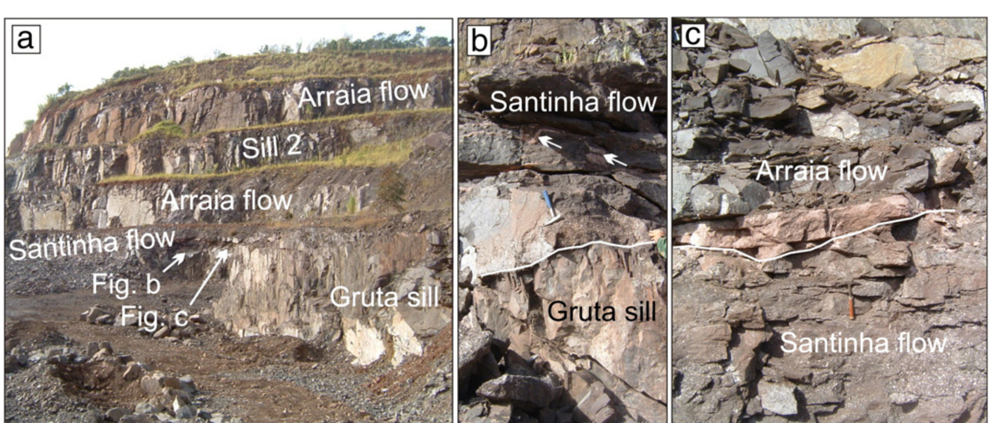

Fig. 10. Field photos of Graxaim quarry. (a) General view showing the position of the Santinha flow below the Arraia flow and of two sills; (b) Gruta sill intrusive into the base of upper amygdaloidal crust of Santinha flow, with sandstone injectites indicated by white arrows; (c) close view of the contact between amygdaloidal upper crust of the Santinha flow and massive overlying Arraia flow, with a sandstone layer (flow) above the top of the Santinha flow. The top of the flow is marked by a white line.

Table 3
Chemical composition of massive and amygdaloidal rocks from the Torres hills and from the Graxaim quarry (BR1C, BR1E). Amygdaloidal lower crust (T4G, T5A, T5A1), massive core (T5C, T5C1). Sample BR1E from amygdaloidal crust. Arraia flow samples from lower (T4C) and upper (T4E) massive cores. Viola sill samples are massive. Santinha flow samples from the Farol Hill, except BR1E (Graxaim quarry). Arraia flow samples from the Furnas hill, except BR1C (Graxaim quarry). Viola sill samples from the Cabras hill (T1A, T1B, T3, T1C), Guarita hill (T2B, T2C) and Furnas hill (T4F1, T4F).

	Santinha flow					Arraia flow					Viola sill							
	T5A	T5A1	T5C1	T5C	BR1E	T4C	T4G	T4E1	T4E	BR1C	T1A	T1B	T2B	T3	T1C	T4F1	T2C	T4F
SiO_2	53.83	53.97	52.52	52.51	50.61	59.91	51.11	59.00	59.38	58.93	56.11	57.26	56.3	56.69	55.61	55.36	55.90	55.62
TiO_2	1.26	1.25	1.34	1.34	1.29	1.39	1.51	1.45	1.39	1.38	1.56	1.56	1.59	1.54	1.58	1.53	1.60	1.54
Al_2O_3	14.05	13.82	14.23	14.47	14.06	13.1	14.70	13.13	13.23	13.36	12.84	12.77	12.69	12.77	12.97	12.98	12.94	12.98
Fe_2O_3	10.25	10.62	11.46	11.40	11.28	10.37	11.82	10.80	10.17	10.38	13.15	13.28	13.19	13.06	13.44	13.18	13.18	13.04
MgO	4.21	4.35	4.66	4.68	4.91	2.50	5.00	2.49	2.73	2.63	2.71	2.70	2.98	2.82	3.18	3.27	3.09	3.25
CaO	5.61	4.94	6.04	5.44	8.45	5.32	2.74	4.18	4.11	5.82	6.03	6.23	6.07	5.83	6.47	7.32	6.27	7.35
Na_2O	3.20	3.22	2.96	3.43	2.65	2.90	5.68	3.24	3.43	2.66	2.64	2.60	2.68	2.29	2.59	2.49	2.56	2.48
K_2O	3.50	1.02	1.01	3.70	0.85	2.89	1.09	1.24	3.14	2.64	2.44	2.36	2.17	2.89	2.17	1.18	2.18	1.21
P_2O_5	0.22	0.22	0.21	0.22	0.22	0.27	0.26	0.27	0.26	0.25	0.23	0.23	0.23	0.23	0.23	0.22	0.23	0.22
MnO	0.15	0.12	0.16	0.16	0.16	0.14	0.13	0.11	0.11	0.15	0.13	0.17	0.17	0.13	0.18	0.19	0.19	0.20
Cr_2O_3	0.004	0.003	0.004	0.003	0.012	–	0.004	–	–	0.004	–	–	–	0.002	–	–	–	0.002
LOI	3.5	3.6	2.5	2.3	5.3	1.0	5.6	1.8	1.8	1.6	1.6	0.6	1.7	1.5	1.3	1.8	1.3	1.9
Sum	99.74	99.66	99.67	99.64	99.77	99.78	99.77	99.77	99.77	99.78	99.43	99.77	99.77	99.77	99.74	99.75	99.74	99.75
Ni	41	40	42	51	57	–	59	–	20	23	30	23	23	–	–	23	20	29
Sc	31	32	36	36	35	28	38	28	27	29	34	34	35	35	36	36	35	35
Ba	639	1112	1084	1415	307	564	235	548	712	549	479	485	451	484	429	393	424	436
Be	1	1	–	1	1	2	–	–	2	2	1	2	1	2	1	–	1	2
Co	34.7	34.4	39.1	38.7	38.2	28.4	47.1	25.5	28.1	31.1	40.5	40.8	41.6	36.0	39.4	39.1	38.2	42.8
Cs	2.7	2.6	1.7	2.0	0.8	1.7	0.1	1.4	2.4	1.6	2.0	2.1	1.9	1.7	2.0	3.9	2.0	5.0
Ga	17.1	15.8	15.6	16.3	16.4	17.9	20.5	17.1	18.1	18.0	19.0	19.0	19.9	18.4	20.2	18.2	18.6	19.1
Hf	4.2	4.2	4.8	4.8	4.6	5.6	4.8	5.6	5.8	5.3	4.8	4.8	5.2	5.2	5.2	4.6	4.9	4.9
Nb	12.6	12.2	12.0	11.3	13.1	15.2	12.3	15.1	14.7	14.9	13.5	13.3	13.5	13.1	13.2	12.0	13.4	13.4
Rb	111	124	109	130	27	112	34	98	117	96	94	91	85	104	71	79	71	89
Sn	2	2	2	2	1	2	2	–	2	2	2	2	2	2	–	–	3	2
Sr	308	373	199	203	294	219	83.4	191	189	215	184	184	186	179	196	230	186	254
Ta	0.8	0.9	0.7	0.9	0.8	1.1	0.9	1.0	1.0	1.0	1.0	0.9	0.9	1.0	0.9	0.8	1.0	0.8
Th	5.7	6.4	5.4	6.1	6.1	9.3	7.1	8.7	9.1	8.8	7.9	6.9	7.9	7.8	7.2	7.3	8.6	7.2
U	1.6	1.8	1.5	1.5	1.0	2.4	2.0	2.0	2.2	2	1.9	1.9	1.8	1.8	1.8	1.6	1.7	1.8
V	275	267	296	316	250	257	311	267	250	317	463	403	406	399	407	374	409	415
W	0.5	0.7	–	–	0.5	1.6	–	–	0.8	0.8	0.9	0.8	0.8	1.1	–	–	–	2.7
Zr	163	171	171	162	169	209	171	196	205	197	185	179	182	182	175	163	176	180
Y	27.9	28.8	26.8	28.9	29.0	33.8	28.2	32.5	36.2	34.2	33.1	33.5	31.6	35.1	30.9	30.4	30.6	34.4
La	24.4	27.8	23.9	23.3	25.0	31.9	24.5	33.1	33.5	31.5	26.9	26.4	24.5	27.7	25.2	24.5	25.2	26.4
Ce	56.5	59.0	59.5	49.9	57.2	73.2	52.2	66.2	75.7	72.3	62.0	62.1	60.4	64.4	54.4	51.4	54.5	62.0
Pr	6.54	6.91	6.34	6.12	6.48	8.68	6.41	8.23	8.60	8.27	7.28	7.21	7.07	7.50	6.67	6.27	6.60	7.17
Nd	26.5	27.5	26.8	26.9	26.4	33.1	27.2	32.6	33.9	33.1	28.4	30.2	27.9	29.4	26.6	25.7	26.8	28.2
Sm	5.35	5.47	5.26	5.04	5.53	6.72	5.82	7.00	6.87	6.67	6.15	6.12	5.85	6.30	6.20	5.64	5.81	6.19
Eu	1.38	1.45	1.42	1.43	1.40	1.61	1.48	1.62	1.59	1.55	1.52	1.55	1.46	1.57	1.52	1.43	1.47	1.55
Gd	5.29	5.65	5.48	5.30	5.41	6.56	5.84	6.70	6.88	6.50	6.20	6.36	5.85	6.64	6.19	5.91	5.92	6.22
Tb	0.87	0.87	0.87	0.89	0.90	1.05	0.99	1.13	1.05	1.05	1.00	1.03	0.98	1.05	1.05	1.00	1.01	1.05
Dy	4.97	4.67	4.90	4.76	5.04	5.90	5.48	6.03	6.10	5.82	6.12	5.84	5.74	6.02	5.96	5.76	5.75	5.97
Ho	1.00	1.02	1.01	1.05	1.01	1.18	1.09	1.24	1.17	1.18	1.18	1.19	1.13	1.18	1.15	1.18	1.11	1.22
Er	2.91	3.04	2.57	2.82	2.95	3.43	3.00	3.40	3.36	3.46	3.39	3.47	3.23	3.40	3.37	3.13	3.19	3.48
Tm	0.43	0.45	0.40	0.44	0.44	0.49	0.47	0.50	0.49	0.49	0.49	0.49	0.49	0.52	0.50	0.46	0.49	0.53
Yb	2.60	2.78	2.60	2.85	2.69	3.18	3.09	3.22	3.07	3.08	3.22	3.03	3.17	3.21	3.18	3.05	3.22	3.19
Lu	0.38	0.39	0.39	0.42	0.41	0.47	0.44	0.46	0.47	0.49	0.48	0.47	0.49	0.48	0.46	0.45	0.46	0.49
Mo	0.3	0.3	0.8	0.7	0.5	0.7	0.6	0.9	0.8	0.4	0.6	0.8	0.7	0.6	1.0	0.5	0.7	0.5
Pb	8.9	8.7	4.1	4.7	9.3	9.3	11.4	6.9	6.0	5.4	4.4	4.8	3.1	3.0	3.4	3.9	3.4	2.1
Zn	58	63	74	72	61	63	99	69	72	59	62	54	70	55	75	41	73	31
Ni	17	15	23	26	37	7	49	9.0	10	8.5	13	12	15	9	12	7	13	6
Au	3.6	0.6	–	–	1.9	0.9	–	–	–	1.4	1.1	1.7	1.4	1.6	1.1	0.7	1.0	3.7
Cu	93	93	143	155	167	55	138	83	80	51	126	175	152	45	155	156	143	158

Fe_2O_3 = total iron; (–) = below detection limit, 0.002 for Cr_2O_3; 20 for Ni; 1 for Sc, Be, and Sn; 0.5 for W; 0.5 ppb for Au. As, Cd, Sb, Bi, Ag, Hg, Tl, Se, and S below detection limit. Oxides in wt.%, trace elements in ppm, except Au in ppb.

4. Results

4.1. Geochemistry

The use of rock geochemistry and scintillometry is essential for the elucidation of volcanic and hydrothermal processes active during the Cretaceous in the Torres region. We analyzed 41 rock samples (Tables 3, 4, 5), including two samples of sandstones from Torres hills and two from the Graxaim quarry, 11 samples of breccia clasts and 26 samples of volcanic and sub-volcanic rocks from Torres hills and Graxaim quarry. The sandstones have higher K_2O than Botucatu Formation samples from Uruguay (Morteani et al., 2010). All volcanic and sub-volcanic rocks are low-TiO_2 (below 2 wt.%), Gramado type (Peate et al., 1992).

The rocks from the Cabras and Guarita hills are geochemically similar (3, 11) and are andesite (57 wt.% SiO_2). This here named Viola sill is geochemically equivalent to the andesite unit at the top of Furnas hill; both have ~1.55 TiO_2 and similar compositions for many trace elements. Differences in MgO and CaO can be ascribed to fractionation in the magma chamber and to the intense hydrothermal alteration.

The Arraia flow present in the Furnas hill is an andesite and has a different TiO_2 content (~1.40 wt.%) from the Viola sill (1.55 wt.%). In

Table 4
Chemical composition of samples from the Graxaim quarry and the Torres hills Botucatu Formation and silicified sandstone layer, sills and dike. Two samples from Graxaim quarry are in Table 5. Samples from the Graxaim quarry: BR1G — sill 2 that evolves to dike; BR1D — sill 1 (Gruta) above and intruded by the sill BR1G; BR1B — sill 2, near the top of the quarry, below sample BR1C (Arraia flow); BR1A — massive flow at the base of the quarry, similar to BR1C (Arraia flow); BR1F — sandstone layer below amygdaloidal flow, intruded by sill 1; BR1H — sandstone layer. Samples from Torres hills: T4A — sandstone layer at the base of breccia 1 and Arraia flow; T2A — sandstone, Botucatu Formation; T5D — sill at sea level, below Santinha flow; T5E — thin (20 cm) dike in lower crust of Santinha flow; T5F — sill at the Gruta da Santinha, below the core type II of Santinha flow.

	Graxaim quarry						Torres hills				
	BR1G	BR1D	BR1B	BR1A	BR1F	BR1H	T4A	T2A	T5D	T5E	T5F
SiO_2	52.31	53.39	52.03	58.12	78.66	82.12	83.17	88.39	50.69	50.71	51.58
TiO_2	1.47	1.44	1.51	1.40	0.17	0.07	0.14	0.06	1.44	1.46	1.40
Al_2O_3	12.90	13.39	13.07	13.32	9.24	6.54	7.75	5.84	13.8	13.74	13.63
Fe_2O_3	13.55	13.15	13.91	10.75	0.87	0.61	1.27	0.78	13.15	12.71	12.82
MgO	4.77	4.61	4.94	2.91	0.12	0.03	0.36	0.05	5.27	5.65	4.91
CaO	8.89	8.12	9.11	6.18	4.54	5.01	1.03	0.07	7.16	6.50	7.87
Na_2O	2.56	2.61	2.60	2.68	0.52	0.16	1.80	1.15	3.20	3.44	2.37
K_2O	1.12	1.50	1.12	2.64	0.33	0.16	2.46	2.75	1.19	1.16	1.12
P_2O_5	0.18	0.20	0.18	0.25	0.06	0.06	0.08	0.03	0.19	0.19	0.19
MnO	0.19	0.19	0.21	0.15	0.02	0.03	0.03	0.01	0.25	0.17	0.21
Cr_2O_3	0.003	0.003	0.003	–	–	–	–	–	0.003	–	0.003
LOI	1.8	1.2	1.1	1.4	5.5	5.2	1.9	0.9	2.9	3.3	3.2
Sum	99.77	99.77	99.75	99.78	100.01	100.02	99.97	99.98	99.70	99.67	99.70
Ni	26	33	31	–	–	–	–	–	33	35	32
Sc	37	34	37	29	2	–	2	–	36	36	36
Ba	295	356	347	525	46	21	410	505	472	554	447
Be	1	1	1	2	–	–	–	–	2	1	–
Co	42.1	42.1	44.7	31.7	1.7	0.9	2.6	2.0	38.7	41.6	41.3
Cs	1.7	1.2	1.5	1.9	6.5	3.2	1.2	1.3	0.8	0.4	1.9
Ga	18.7	20.0	19.3	20.6	16.3	10.6	7.1	4.8	20.7	18.6	19.2
Hf	4.0	4.4	3.9	5.7	3.1	1.4	1.7	1.6	4.7	4.2	3.9
Nb	9.3	12.9	9.1	14.5	3.9	2.3	4.9	1.9	11.4	12.1	10.6
Rb	49	55	35	99	13	7	62	83	49	58	41
Sn	1	2	1	3	–	–	–	–	2	2	2
Sr	222	224	225	214	50	26	85	57	301	234	348
Ta	0.5	0.8	0.5	1.0	0.3	0.2	0.9	0.3	0.8	0.8	0.8
Th	4.5	6.2	4.6	8.8	2.2	2.0	2.4	2.3	7.2	5.7	5.4
U	0.7	1.4	0.7	2.2	0.6	0.6	0.7	0.7	1.4	1.5	1.4
V	377	365	404	283	13	10	43	8	378	408	401
W	–	0.5	–	0.7	–	–	0.8	–	0.6	0.8	–
Zr	143	156	144	195	131	46	53	58	151	158	148
Y	32.0	31.7	32.3	32.3	8.1	6.8	9.1	6.2	33.0	32.3	29.7
La	19.5	23.1	20.6	31.1	5.9	6.5	10.1	5.8	21.9	23.0	21.0
Ce	45.3	53.5	46.5	73.2	15.3	15.7	18.6	14.9	50.1	55.5	49.7
Pr	5.34	6.12	5.47	8.26	1.83	1.83	2.37	1.67	5.74	5.90	5.55
Nd	22.5	25.4	23.1	33.4	7.2	7.6	9.0	6.6	22.2	24.3	21.5
Sm	5.00	5.39	5.11	6.59	1.58	1.39	1.91	1.32	4.94	5.20	4.71
Eu	1.40	1.48	1.46	1.54	0.47	0.47	0.57	0.44	1.51	1.49	1.42
Gd	5.58	5.73	5.71	6.59	1.44	1.27	1.68	1.21	5.64	5.65	5.12
Tb	0.95	0.94	0.96	1.04	0.25	0.21	0.28	0.20	1.01	1.02	0.93
Dy	5.69	5.52	5.53	5.81	1.40	1.17	1.60	1.13	5.46	5.28	5.15
Ho	1.13	1.12	1.15	1.17	0.29	0.24	0.31	0.21	1.19	1.16	1.12
Er	3.41	3.29	3.4	3.27	0.90	0.72	0.93	0.63	3.31	3.32	3.00
Tm	0.50	0.47	0.51	0.49	0.13	0.11	0.14	0.10	0.49	0.51	0.45
Yb	3.03	2.96	3.00	3.05	0.83	0.61	0.85	0.63	3.00	2.97	2.98
Lu	0.46	0.44	0.47	0.47	0.14	0.10	0.14	0.09	0.45	0.43	0.42
Mo	0.4	0.6	0.6	0.5	0.3	0.2	0.3	0.2	0.8	0.9	0.7
Pb	3.7	2.6	1.8	5.7	3.3	2.3	9.8	3.5	6.9	9.8	5.8
Zn	43	64	53	44	3	2	2	2	69	109	58
Ni	7.0	11.5	10.8	7.4	2.0	1.6	3.2	2.0	7.8	13.3	8.0
Au	–	2.8	–	–	–	–	1.6	3.3	1.8	1.1	2.2
Cu	79	99	157	66	21	74	6	3	160	222	154

Fe_2O_3 = total iron; (–) = below detection limit, 0.002 for Cr_2O_3; 20 for Ni; 1 for Sc, Be, Sn; 0.5 for W; 0.5 ppb for Au. The contents of As, Cd, Sb, Bi, Ag, Hg, Tl, Se, C, are S are below detection limit. Oxides in wt.%, trace elements in ppm, except Au in ppb.

short, the two southernmost Cabras and Guarita hills are andesite (Viola sill), whereas Furnas hill is a succession of one lava flow at the base, succeeded on top by the Viola sill.

The Farol hill is at the sea level just as the other three hills, but it is composed of a lava flow that is not present in the other hills. Two samples were analyzed from the massive core type II of the lava and have low LOI (~2.0 wt.%); they are considered representative of the chemical composition of the lava in terms of the least mobile trace elements. The SiO_2 content (53.83 wt.%, basaltic andesite) of this Santinha flow is taken from sample T5A, the lower amygdaloidal crust. The content of TiO_2 (1.25 wt.%) is similar in the analyzed samples, including T5B (breccia 3). K_2O, Rb and Sr are much lower in T5B, but this is probably due to the high LOI of the sample.

In the Graxaim quarry, sample BR1E (crust at the bottom of the quarry) has similar composition to the Santinha flow, and sample BR1C (crust at the top of the quarry) is chemically similar to the samples from the Arraia flow (Fig. 11). The correlation of the two lava flows between the Graxaim quarry and the Furnas and Cabras hills suggests that the Santinha flow underlies the Arraia flow in both places although it is not exposed in Torres.

Overall, the crusts have similar chemical composition to the corresponding core of the same flow. On the other hand, the composition

Table 5
Chemical analyses of breccia volcanic clasts from Torres hills. Arraia flow breccias 1 and 2 are from the Furnas hill, Santinha flow breccia 3 is from Farol hill.

	Arraia flow, lower breccia 1				Arraia flow, upper breccia 2				Santinha flow, breccia 3		
	B1A	B1B	T4B	B1C	B2A	B2B	B2C	T4D	T5B1	T5B2	T5B
SiO_2	50.62	44.28	49.01	57.93	53.53	55.88	58.00	54.91	51.72	51.73	52.03
TiO_2	1.56	0.75	1.75	1.46	1.66	1.5	1.49	1.75	1.61	1.42	1.20
Al_2O_3	14.15	9.36	14.14	13.61	14.2	14.4	13.51	15.3	12.76	14.14	13.49
Fe_2O_3	12.22	8.46	13.67	10.69	12.04	10.63	10.94	9.86	13.1	11.35	10.59
MgO	5.29	2.06	5.27	1.86	3.21	2.56	2.13	2.87	2.62	3.53	4.99
CaO	3.18	15.92	2.34	1.81	3.11	2.8	3.22	2.01	4.74	4.85	5.14
Na_2O	4.72	3.4	4.63	4.55	3.82	5.72	4.95	6.4	4.06	5.1	4.4
K_2O	2.43	1.31	2.21	3.36	5.12	3.1	3.1	2.02	1.24	1.17	1.95
P_2O_5	0.26	0.13	0.33	0.27	0.32	0.29	0.29	0.33	0.28	0.27	0.22
MnO	0.13	0.69	0.21	0.12	0.18	0.14	0.13	0.33	0.11	0.12	0.15
Cr_2O_3	0.002	0.002	0.003	–	–	–	–	–	0.003	0.002	0.004
LOI	5.1	13.5	6.1	4.0	2.5	2.7	2.0	4.0	3.1	5.0	5.6
Sum	99.7	99.86	99.7	99.66	99.68	99.74	99.75	99.78	99.64	99.77	99.78
Ni	57	39	31	31	33	26	26	–	22	40	38
Sc	39	24	36	29	33	29	29	33	42	37	31
Ba	659	314	549	1295	1015	754	899	400	1176	418	355
Be	2	2	1	3	2	2	2	2	–	2	1
Co	48.0	23.8	42.0	31.3	38.0	31.6	27.5	31.2	24.0	39.8	38.5
Cs	0.6	0.5	0.7	1.1	0.8	2.7	2.2	2.4	0.8	3.1	1.5
Ga	20.2	10.4	23.0	18.0	16.5	16.2	12.0	22.3	9.3	15.7	17.8
Hf	5.8	2.3	6.2	6.6	6.4	6.1	6.5	7.3	6.0	4.4	4.4
Nb	14.4	6.3	17.7	16.3	16.7	16.4	17.2	19.1	15.3	13.0	11.0
Rb	72	30	68	111	144	127	113	66	150	54	54
Sn	2	1	3	3	3	3	3	3	3	2	2
Sr	121	96	99	142	149	179	158	124	65	83	64
Ta	1.0	0.5	1.0	1.0	1.1	1.3	1.1	1.4	1.1	0.8	0.7
Th	7.5	3.5	10.1	11.1	10.1	10.2	9.8	11.7	8.0	6.6	5.9
U	2.3	0.9	2.9	2.4	2.8	2.4	2.5	2.8	2.5	3.6	2.0
V	366	205	367	276	382	303	320	290	747	297	283
W	1.2	–	1.5	0.6	1.0	0.9	1.3	0.6	1.7	1.1	0.8
Zr	201	89	233	227	231	231	234	258	223	178	155
Y	33.0	18.9	38.7	110.1	37.1	35.9	36.1	37.4	30.8	33.3	28.1
La	26.8	20.1	32.7	131.0	30.7	38.9	39.2	30.7	36.5	30.9	20.1
Ce	63.9	32.2	82.4	104.8	71.1	81.0	79.9	84.4	82.9	71.8	52.7
Pr	7.76	3.8	9.52	29.86	8.74	9.5	9.53	10.26	8.88	7.87	6.3
Nd	32.5	16.1	38.4	119.2	35.4	37.7	38.1	41.0	37.6	33.6	25.4
Sm	6.37	3.27	7.67	21.78	7.23	7.39	7.41	8.07	6.61	6.12	5.12
Eu	1.68	0.82	1.94	5.13	1.73	1.76	1.71	1.66	1.67	1.69	1.32
Gd	6.29	3.29	7.56	23.1	7.2	7.11	7.06	8.04	6.75	6.48	5.18
Tb	1.05	0.55	1.24	3.75	1.17	1.16	1.15	1.27	1.1	1.05	0.86
Dy	5.7	3.14	6.96	20.71	6.42	6.57	6.46	7.2	6.01	5.47	4.71
Ho	1.19	0.66	1.37	4.07	1.32	1.27	1.28	1.38	1.24	1.17	0.95
Er	3.27	1.93	3.94	11.01	3.71	3.59	3.71	3.94	3.4	3.19	2.81
Tm	0.48	0.29	0.58	1.59	0.56	0.53	0.53	0.59	0.53	0.47	0.4
Yb	3.07	1.87	3.69	9.15	3.53	3.34	3.31	3.68	3.28	2.8	2.48
Lu	0.45	0.29	0.57	1.3	0.54	0.5	0.49	0.56	0.44	0.43	0.38
Mo	0.7	0.5	0.9	0.4	1.1	0.7	1.0	1.1	0.8	0.8	0.7
Pb	11.7	13.2	16.3	13.2	9.7	10.5	12.3	12.4	13.5	10.7	10.5
Zn	136	23	130	101	112	78	88	140	36	65	87
Ni	34.9	23.3	29.6	23.7	17.1	15.4	14.9	20.4	18.1	25.3	27.3
Au	0.6	0.7	0.9	1.0	1.3	1.1	1.2	–	–	–	–
Cu	125	69	126	73	133	77	67	97	101	109	73

Fe_2O_3 = total iron; (–) = below detection limit, 0.002 for Cr_2O_3; 20 for Ni; 1 for Sc, Be, and Sn; 0.5 for W; 0.5 ppb for Au; As, Cd, Sb, Bi, Ag, Hg, Tl, Se, and S below (or near) detection limit. Oxides in wt.%, trace elements in ppm, except Au in ppb.

of the clasts varies considerably. A trend is present towards enrichment in less-mobile elements in the clasts (star in Fig. 12); e.g., TiO_2, P_2O_5, Zr, U, Th, Y and a strong depletion in CaO.

4.2. Scintillometry

Scintillometric measurements were made in outcropping rocks from all hills and the Graxaim quarry (Table 6), displaying a total variation of 65–138 cps. The rate of emission is dependent upon the concentration of K_2O, U and Th in the rock; it is thus an identifying property of each magma, but hydrothermal processes may have modified the chemistry of the rock, leading particularly to a decrease in SiO_2, K_2O and Rb and oscillation in MgO, CaO and some other elements (e.g., Hartmann et al., 2010a). U and Th can also be mobilized in hydrothermal fluids and thus contribute to variation in scintillometric measurements.

Each lava flow or sill has characteristic cps values (Table 6). The Botucatu Formation sandstones have 100 cps (Table 6) that is higher than in other parts of the formation, due to higher K_2O content (2.75 wt.%). In Artigas, Uruguay, the sandstones only have 0.33 wt.% K_2O and a correspondingly low 40 cps (Hartmann et al., 2010a; Morteani et al., 2010). Clast-dominated breccia 1 has 90 cps. Above it, the Arraia flow has 130 cps. The Viola lava layer on top of the Furnas hill has only 65 cps (readings on small exposures), but is considered the equivalent of the Guarita sill (120 cps). The Santinha flow has 110 cps, breccia 3 only 90 cps, although the clasts have similar chemical composition as the flow. Overall, scintillometry is helpful in the field identification of each lava unit and the establishment of

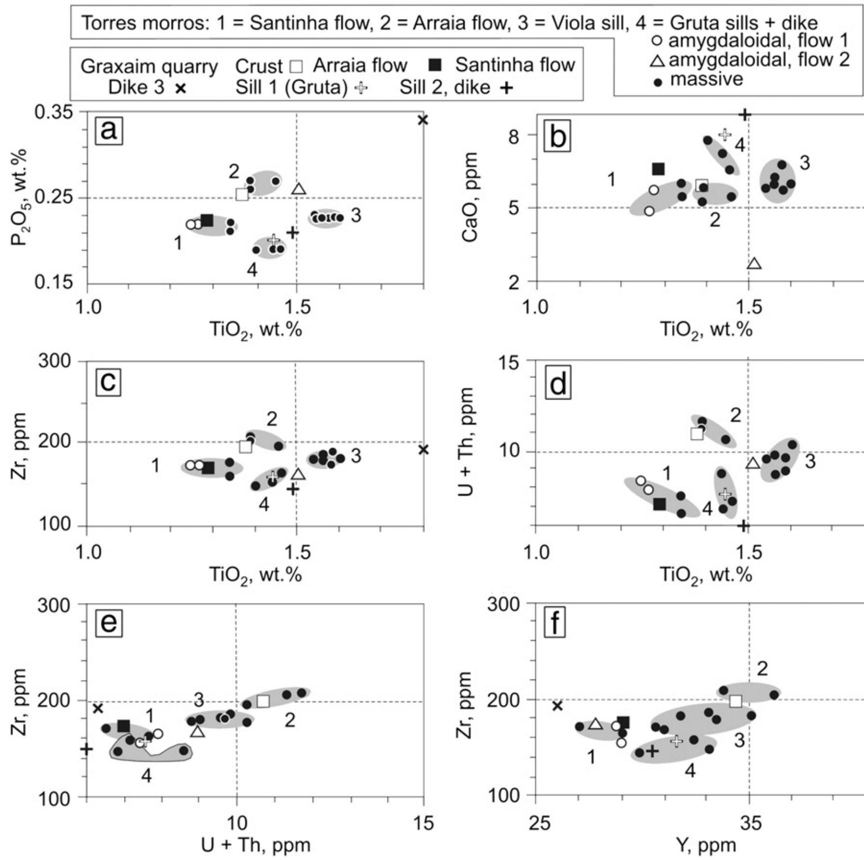

Fig. 11. Trace element diagrams displaying the presence of two lava flows in the Torres region. Correlation of flows, dikes and sills between Graxaim quarry and Torres indicated.

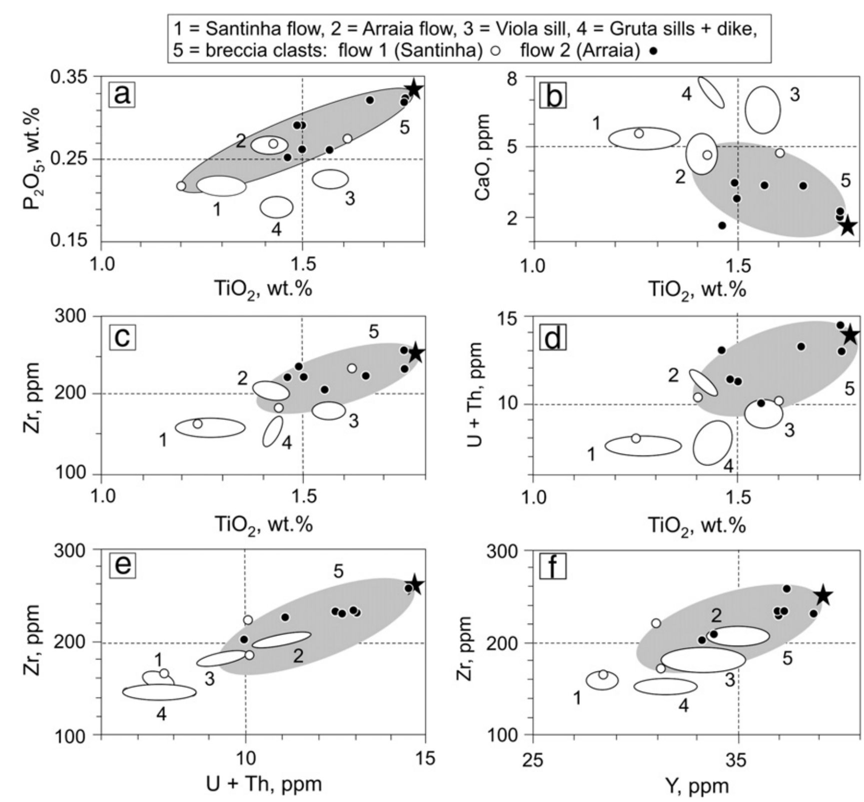

Fig. 12. Trace element diagrams of Torres breccia clasts, indicating geochemical mobility of elements during hydrothermal alteration. Compositional fields of rocks from Fig. 11 indicated as blank, circled areas.

Table 6
Scintillometric measurements in outcrops of volcanic rocks from Torres hills. (–) = not measured; cps = counts per second (total emission rate from U, Th, K); n = number of measurements; av. = average; s.d. = standard deviation; sample numbers correspond to location of measurement; T1C — northern top of Morro das Cabras; T4G — amygdaloidal breccia 1; T5D — sill at sea level at the Gruta da Santinha; T5F — sill above Gruta da Santinha.

Outcrops	Rock type	n	av. (s.d.)
Cabras hill			
T1A, T1B	Andesite	12	114 (8.7)
T1C	–	12	128 (13.5)
Guarita hill			
T2A	Sandstone	6	95 (2.2)
T2B	Sandstone	12	122 (9.2)
Furnas hill			
vT4A	Sandstone	12	62 (1.8)
T4B	Andesite	11	98 (5.0)
T4C	Andesite	12	138 (10.3)
T4D	Andesite	10	99 (7.9)
T4E	Andesite	11	127 (31.9)
T4F	Basaltic andesite	13	69 (4.5)
T4G	–	12	120 (2.6)
Farol hill			
T5A	Basaltic andesite	10	101 (3.9)
T5B	Basaltic andesite	11	81 (7.0)
T5C	Basaltic andesite	11	103 (7.6)
T5D	Basalt	14	85 (2.8)
T5F	Basalt	12	95 (4.9)

the lava stratigraphy, particularly after the geochemical analyses of the rocks (Fig. 13).

5. Interpretation

The integrated knowledge acquired from field relationships, rock geochemistry and scintillometry leads to a better understanding of the Cretaceous geological evolution of the Torres region, particularly the sequence of volcanic processes and the hydrothermal interaction of buried, loose, desert dune sand with basaltic rocks in a low-temperature environment. The hydrothermal breccias were formed by hydrofracturing of cold volcanic rocks by highly pressured

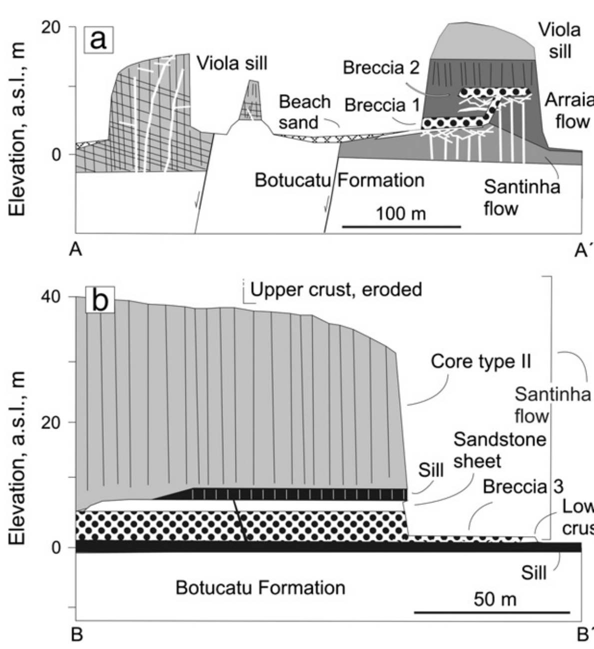

Fig. 13. Two stratigraphic sections, as located in Fig. 2. Unconstrained extension below land or sea surface. (a) Botucatu Formation, Guarita sill, several lava flows and breccias 1 and 2; (b) lava flows and position of breccia and massive sandstone between amygdaloidal lower crust and the base of core type II.

hydrothermal fluids, as conceptually summarized in New World Encyclopedia (www.newworldencyclopedia.org/entry/Breccia). Breccia 2 is here interpreted as a breccia sill forcefully intruded into the cold core of the Arraia flow.

Only a thin portion of the top (5 m) of the Botucatu Formation (commonly 100 m thick) is exposed in Torres and is directly in contact with the injected Viola sill. However, drilling is required to test the alternative hypothesis that the paleodunes are part of an intertrap unit, not the top of the Botucatu Formation. The high-angle, cross-bedding of the sandstones at the base of the Guarita hill outcrop indicates the eolian, desert origin of the paleodune (Scherer, 2000; Petry et al., 2007). This formation, and to a lesser degree the underlying Guará Formation, constitutes since the Cretaceous the huge Guarani aquifer (Araújo et al., 1999), that extends under the entire extent of the Serra Geral Group, encompassing approximately 1,200,000 km^2 with few gaps. This aquifer is one of the largest in the world. The presence of this aquifer makes the Paraná volcanic province unique, because the other large continental volcanic provinces (e.g., Columbia River in the USA, Karoo in South Africa, Deccan in India) have weak aquifers below the volcanic rocks. For comparison, one of the largest and most productive aquifers within the United States is the eastern Snake River Plain aquifer, Idaho, contains voluminous basalts but has a complex structure and is predominantly unconfined (Mazurek, 2004).

The water table is close to the surface in present-day deserts, e.g., Sahara and Kalahari. Filling of the aquifer after burial by the first lava flow probably occurred in a short time, perhaps thousands of years (Hartmann et al., 2012). Heating of the aquifer by residual heat from every individual volcanic pulse established the scene for the intense hydrothermal processes that left their imprint in the Serra Geral Group, including the Torres rocks. More extensive evaluation of the protracted processes of lava sealing and fault–valve action of the aqueous fluid flow can be found in Hartmann et al. (2012).

The large variation in chemical composition of clasts from the three breccias is interpreted as variable shrinking of the clasts by large volume loss of a few major elements; e.g., CaO, K_2O. The observed enrichment of the clasts in less mobile elements (e.g., Ti, P, Zr, U, Th) is interpreted as caused by leaching of major elements during hydrothermal alteration. As commonly observed in metassomatic rocks, the chemical composition of the clasts tends to become more homogeneous. This is indicated by the star in Fig. 12, a model of the ultimate composition attained by altered clasts. Element mobility seems more extreme than in altered andesitic volcanoes, where Th, Zr, Hf and LREE remain immobile (Salaün et al., 2011).

The crosscutting relationship of the silicified sandstone dikes with the zeolite-filled amygdales in the Graxaim quarry is definitive evidence that sand mobilization occurred in the Torres region after the liquid lava had cooled to less than 130 °C. This concurs with the observations made by Hartmann et al. (2012) over a large extent of the Paraná volcanic province, where the sand intrusions (dike, sill, flow, breccia) are observed to intrude amygdaloidal crusts. Thin (~1 mm) sedimentary dikes are observed to cut amygdales filled with zeolites, so the dikes are younger than the zeolites. Sand injection did not occur during lava effusion (~1150 °C), therefore. Clinoptilolite–heulandite and mordenite are common in Serra Geral Group amygdales (Duarte et al., 2009; Hartmann et al., 2012); in Iceland, this hydrothermal assemblage yields temperatures of 110–120 °C (Neuhoff et al., 2006).

The lack of evidence in the Torres region for high-temperature interaction of the dry dune sand with the lavas does not support the interpretations of Petry et al. (2007) who considered the breccias as peperite-like rocks. Phreatomagmatic breccias (e.g., peperites) are formed in situ (Brown and Bell, 2007) by disintegration of magma intruding and mingling with unconsolidated or poorly consolidated, wet sediments. These magma–sediment mixtures are classified as peperites where they occur at the margins of intrusions or at the base of lava flows, as the result of phreatomagmatic processes. Fluidal clasts in peperites tend to dominate the basal facies. It is also known that phreatomagmatic explosions are common in basaltic effusions over water-saturated sediments (e.g., Belousov et al., 2011). Glassy or quench-textured rims occur in clasts of classical peperites, and these were neither described nor encountered in the Torres breccias. Contact metamorphic effects are expected (Mazurek, 2004), because "most of the peperitic packages … contain amoeboid basalt clasts with fluidal margins … floating in a hard, baked sediment matrix. The fluidal margined basalt clasts along gradational contact margins with sedimentary interbeds are amoeboid-looking to the naked eye…".

In the absence of water-saturated sediments to form peperites, breccias similar to those here described can be generated by hydrothermal (phreatic) processes. Sand can be mobilized into a caprock after it is fluidized in water or oil (Hurst et al., 2011); in the present case, water and its vapor. Dry sand cannot be mobilized upwards into an overlying, cool lava flow because of friction resistance. Presently-observed sand dikes, sills and flows were actually water dikes, sills and flows. After turbulent flow ceased, the sand settled out of the water. Sedimentary structures similar to other water-laid sand bodies can be formed, such as cross-bedding, layering and graded bedding. The volumetric proportion is commonly 30% sand which is fluidized in 70% water. The mechanical properties of sand-carrying water are comparable to basaltic lavas, and this explains the great similarity in geological relationships of dikes and sills of sand and basalt.

In active systems in Israel that may be comparable to the sand intrusion processes in the Torres region, analytical models indicate that clastic dikes are propagated under turbulent flow conditions and velocities of 4–65 m/s and driving pressures of 1–2 MPa (Levi et al., 2011). Experimental studies indicate that sand is mobilized by turbulent flow at minimum velocities 0.3–0.4 m/s (Johari and Taib, 2007). After turbulent flow ceased in Torres, the sand was deposited in the water-filled, open cavities; water later dissipated, only sand remaining as a dike. Continued fluid flow in Torres during the Cretaceous caused the intense silicification of the dike into a hard sandstone. The availability of a large volume of water in the Guarani aquifer led to the intense silicification of the injected sandstone dikes.

Thermal recrystallization would be expected to occur in loose sand composed of approximately 82% quartz, 16% feldspar, 2% lithic fragments (Petry et al., 2007), 2.75 wt.% K_2O (this work) when it is immersed and remains in close contact for a few months with andesite lava at 1150 °C. In the studied region, the silicified sandstone from dikes and breccias is made up of unrecrystallized detrital grains; quartz is partly corroded and immersed in a chalcedony cement. No evidence of thermal metamorphism is observed, such as recrystallization of the detrital grains. Thus, the presented data lead us to interpret that the sandstone, which was a loose sand at the time of volcanism, was not exposed to the high temperatures in the interior of liquid andesite lava (1150 °C).

The geology of Torres consists mostly of two lava flows of basaltic andesite and andesite composition, which were affected by intense hydrothermal alteration after solidification and cooling to less than 130 °C (Table 7). These hydrothermal (H) processes are overall similar to those described by Hartmann et al. (2012). Three events (H1, H2, H3) occurred in sequence, intercalated by the formation of two seals. For instance, sealing of faults may occur in two years, as measured in Iceland (Claesson et al., 2007). Immediately after cooling, the lava flows had high porosity (~30 vol.%) and permeability due to the presence of vesicles (event M, magmatic) and fractures. The hot water and vapor originated in the Guarani aquifer (Gilg et al., 2003; Morteani et al., 2010; Duarte et al., 2011; Hartmann et al., 2012) caused the initial alteration of the rocks and the precipitation of zeolites (including clinoptilolite) and smectites in the vesicles and fractures (H1 event). This process sealed the lava flow (seal 1), leading to an increase in the pressure exerted by water vapor and to the generation of related structural features of sand injection (H2). Conditions were thus reached for the formation of hydrothermal breccias, because the presence of an impermeable caprock horizon (a seal) is required for brecciation (Jébrak, 1997; Tamas and Milési, 2003). The continued percolation of hot fluid again sealed the porosity (seal 2) and led to overpressure of vapor, with concomitant ballooning of the smectite andesite forming quartz geodes (e.g., Arraia flow); this event H3 was not intense in the region.

As described by Tamas and Milési (2003), "the fragments participation exceeds the matrix participation in the case of hydrothermal breccias. The most common hydrothermal breccia facies is the clast supported one", although some portions are matrix-supported. The three breccia units in Torres are mostly clast-supported, although some portions are sandstone-supported. The matrix of the breccias, and also the sandstone dikes and sills, are variably cemented by chalcedony; as mentioned by Tamas and Milési (2003), "cement is ubiquitously present in hydrothermal breccias." These authors also mention the close genetic and spatial relationship between boiling and hydrothermal brecciation, because brecciation occurs at the level of boiling of water. In our interpretation, the breccias were formed in Torres in the Cretaceous whenever the ascending hot water and its vapor made

Table 7
Evidence from this investigation or (quotation marks) reinterpreted from Petry et al. (2007) that favor a phreatic origin of the sand dikes, sills and breccias from the Torres hills.

Evidence	Present interpretation
"The horizontal jointing does not propagate into the clastic dike"	Intrusion of sand occurred after the formation of the horizontal jointing in the brittle rock
"Sand intruded the vertically-jointed andesite along the joints"	Lava core was already solid to sustain a sand dike; therefore, brittle
Breccia 1 inside lower amygdaloidal crust	Intrusive phreatic breccia
Breccia 2 below core type II	Intrusive phreatic breccia
Breccia 3 inside and at the top of lower amygdaloidal crust, below core type II	Phreatic origin; phreatomagmatic breccias (e.g., peperite) typically occur at the base of lava flows
Angular clast shape	Phreatic breccia, brittle rock
Mostly clast-supported breccia	Phreatic breccia
Clast rims texturally similar to core, not quenched	Low-temperature contact of clast with sand and water
Clasts are amygdaloidal	Brecciation occurred after degassing of lava; rock was solid; breccia is phreatic
Sand grains spherical, detrital	Grains did not recrystallize during thermal event
Sand grains corroded	Grain corrosion by hot water
Sandstone cement made up of chalcedony	Low-temperature silica precipitation
Sandstone dikes cut zeolite-filled amygdales	Sand was injected at low temperature, after the amygdales were filled with zeolites
Sandstone partly fills zeolite-filled amygdales	Low-temperature fluid dissolved zeolites and carried sand into the amygdale
Quartz geodes in Arraia flow	Low-temperature, hydrothermal process
Lozenge fractures in Viola sill (Cabras and Furnas hills); sand dikes in fractures	Sill was sealed by hydrothermal event (H1) through zeolite and clay mineral precipitation Sand intrusion after doming caused by water vapor overpressure
Narrow (1 cm), sand sills in the Cabras hill	Lifting of hangingwall andesite by water vapor overpressure
Vertical cooling joints in Guaritas sill (Guarita hill); few sand dikes	Water vapor escaped through joints; no overpressure generated for sand fluidization
Sandstone dikes in lozenge fractures in Arraia flow (Furnas hill)	Sand intrusion after doming and lozenge fracturing of rock by water vapor overpressure
Jig-saw clasts in breccia 1	Phreatic brecciation

direct contact with atmospheric pressure, either by doming and fracturing 5–20 m thick overburden or by reaching the base of vertically-jointed, massive core type II.

One feature is the formation of sand dikes and sills, another is the lozenge-shaped fracturing of the sealed flow or sill, and a third is the formation of sandstone–andesite breccias. The breccias were formed in two different positions in the flows, inside the amygdaloidal lower crust (breccia 1) and below the vertical cooling joints of core type II in breccias 2 and 3. Similar breccias below the fracture-permeable core type II were described in the Los Catalanes gemological district and the Quaraí mining district by Hartmann et al. (2012). This may be similar to the description of Tamas and Milési (2003) that “structural control is frequently responsible for the location of phreatic breccia structures”.

During its ascent, the hydrothermal breccia may intrude the country rock, similar to diatremes, so the clasts will have the composition of the underlying volcanic rock affected by brecciation (Tamas and Milési, 2003). We interpret the presence of breccia 2 below the core type II of the Arraia flow as caused by upward injection of hydrothermal breccia that was generated along with breccia 1. Breccia 2 is thus interpreted as a breccia sill.

The cavities (now silicified sandstone dike, sill, breccia and massive sandstone layer) and clastic infills (sand) present in the Torres volcanic rocks may have originated by similar fluid overpressure processes as those described by Walker et al. (2011) in Tertiary basalts in the NE Atlantic margin. They describe “0.1–0.6 m thick sub-horizontal clastic units displaying internal features consistent with deposition from flowing water passing through complex open subterranean cavity systems within fractured basalts and anastomosing millimeter-scale and planar decimeter-scale clastic intrusion features mobilized and emplaced during transient, fault-related overpressuring events along pre-existing fractures cutting the surrounding volcanic units.” In the Santinha breccia 3, the massive sandstone that overlies the breccia is here interpreted as formed in a similar “open subterranean cavity system” generated by fluid overpressure.

The third hydrothermal event (H3) occurred after the lava flow and sill (and sand dikes) were sealed at the end of the second event. H3 also caused continued intense alteration of the andesite into smectite and zeolite. The quartz geodes observed at the top of Furnas hill were formed and filled during H3, in a process described by Hartmann et al. (2012). In the NE Atlantic margin examples of Walker et al. (2011), cavities were opened in volcanic rocks that remain permeable, because sealing of the clastic infills did not occur. H3 in the Torres rocks had weak intensity, because the injected sandstone in the three breccias and the overlying layer at Santinha were poorly silicified.

This interpretation of the geological evolution of the Torres region incorporates all field evidence, integrated with geochemical and scintillometric data, into a single, continuous model of magmatism and sequential hydrothermal alteration. It particularly sheds light into the tectonic processes caused by water vapor overpressure on seal layers, represented in Torres by basaltic andesite and andesite flows. Different from offshore petroleum basins, where the fluids (oil or water) carrying fluidized sand are at a temperature of 20–70 °C, the tectonic processes related to the heated Guarani aquifer occurred at a much higher temperature near 130 °C. At this temperature, water vapor can lift 5–20 m of andesite to generate the observed breccias at the base of the flows, or keep the core type II lifted to make room for an underground river of water (+ sand) and so deposit a sand layer above the breccia.

We have thus described a novel process of loose-sand aquifer interaction with seal basaltic lavas at a much higher hydrothermal temperature than the descriptions in the review of the subject by Hurst et al. (2011). The Paraná volcanic province is one of the largest volcanic sequences in the continents, is underlain by a major sand sea converted into an aquifer and was affected by systematic, flow-by-flow injection of hot water and its vapor. The result is a large number of sand injectites (dikes, sills) and extrudites over the entire vertical and horizontal extent of the province, as here exemplified for the Torres region.

6. Conclusions

The main conclusion of this investigation is that initially dry, desert sand can be mobilized and injected upwards into a sealed volcanic rock after the loose sand had the pores filled with hot water and its vapor. Seismic activity may be required to trigger the fluidization of the sand and the intrusion processes. Sequential heating by pulses of volcanism generated vapor and related tectonic processes such as doming with associated lozenge fracturing of the overlying seal with accompanying sand dike and sill formation. Also, sandstone–andesite breccias were formed by explosion of the vapor at the amygdaloidal lower and upper crusts of the flow and even inside the flow below the vertically-jointed, massive core. Similar to diatremes, hydrothermal breccias intruded overlying flow units as dikes and laterally as sills.

In the Torres region, the two southern hills are the Cabras and Guarita hills, both made up of the Viola sill. The Furnas hill to the north is a sequence of one lava flow (Arraia flow) and the Viola sill on top. The northernmost Farol hill is made up of one lava flow (Santinha flow) and the Gruta sills and dike.

The interaction of heated Guarani aquifer water with cold Paraná volcanic province rocks explains the geological features observed in Torres including the sandstone–andesite breccias, the silicified sandstone layer on top of breccia 3, the dikes and sills of silicified sandstone, the presence of silicified sandstone in lozenge fractures of the andesite, the crosscutting relationship of thin sandstone dikes with zeolite-filled amygdales and the presence of 10–20 cm quartz geodes. No evidence of phreatomagmatic brecciation was observed in Torres. The breccias were formed by phreatic processes at the boiling point of water close to the surface (probably less than 20 m). All three breccia bodies in Torres are hydrothermal, intrusive into two different lava flows.

This is a significant contribution to the understanding of the geological relationships generated in a large continental flood basalt province by hot water and its vapor originated by the repeated heating of a huge freshwater aquifer.

Acknowledgments

This investigation was supported by project of excellence PRONEX FAPERGS/CNPq on “Strategic Minerals from Southern Brazil”, coordinated by Léo A. Hartmann. Karine da Rosa Arena is grateful to FAPERGS for a scholarship. Leonardo Manara Rosenstengel, Juliana Pertille da Silva, Lucas Machado Antunes and Patrick Guimarães are acknowledged for their help during field work. “Secretaria do Meio Ambiente de Torres” kindly permitted the visit to the Parque Guaritas and the collection of rock samples. The Geological Survey of Brazil (CPRM) kindly allowed the use of their portable gamma-ray scintillometer.

References

Araújo, L.M., França, A.B., Potter, P.E., 1999. Hydrogeology of the Mercosul aquifer system in the Paraná and Chaco-Paraná Basins, South America, and comparison with the Navajo-Nugget aquifer system, USA. Hydrogeological Journal 7, 317–336.

Arioli, E.E., Licht, O.A.B., Vasconcellos, E.M.G., Bonnet, K.L., Santos, E.M., 2008. Faciologia vulcânica da Formação Serra Geral na região de Guarapuava, Paraná. IV Simpósio de Vulcanismo e Ambientes Associados, Foz do Iguaçu; Sociedade Brasileira de Geologia, Anais. 6 pp. (CD-ROM).

Belousov, A., Behncke, B., Belousova, M., 2011. Generation of pyroclastic flows by explosive interaction of lava flows with ice/water-saturated substrate. Journal of Volcanology and Geothermal Research 202, 60–72.

Brown, D.J., Bell, B.R., 2007. How do you grade peperites? Journal of Volcanology and Geothermal Research 159, 409–420.

Claesson, L., Skelton, A., Graham, C., Mörth, C.-M., 2007. The timescale and mechanisms of fault sealing and water-rock interaction after an earthquake. Geofluids 7, 427–440.

Duarte, L.C., Hartmann, L.A., Vasconcellos, M.A.Z., Medeiros, J.T.N., Theye, T., 2009. Epigenetic formation of amethyst-bearing geodes from Los Catalanes gemological district, Artigas, Uruguay, southern Paraná Magmatic Province. Journal of Volcanology and Geothermal Research 184, 427–436.

Duarte, L.C., Hartmann, L.A., Ronchi, L.H., Berner, Z., Theye, T., Massone, H.J., 2011. Stable isotope and mineralogical investigation of the genesis of amethyst geodes in the Los Catalanes gemological district, Uruguay, southernmost Paraná volcanic province. Mineralium Deposita 46, 239–255.

Gilg, H.A., Morteani, G., Kostitsyn, Y., Preinfalk, C., Gatter, I., Strieder, A.J., 2003. Genesis of amethyst geodes in basaltic rocks of the Serra Geral Formation (Ametista do Sul, Rio Grande do Sul, Brazil): a fluid inclusion, REE, oxygen, carbon, and Sri sotope study on basalt, quartz, and calcite. Mineralium Deposita 38, 1009–1025.

Hartmann, L.A., Wildner, W., Duarte, L.C., Duarte, S.K., Pertille, J., Arena, K.R., Martins, L.C., Dias, N.L., 2010a. Geochemical and scintillometric characterization and correlation of amethyst geode-bearing Paraná lavas from the Quaraí and Los Catalanes districts, Brazil and Uruguay. Geological Magazine 147, 954–970.

Hartmann, L.A., Duarte, S.K., Pertille, J., 2010b. Roteiro de Campo. Geologia dos geodos de ametista de Quaraí. Brasil-Uma imersão no vulcanismo, hidrotermalismo e na exploração mineral no Grupo Serra Geral. Porto Alegre, Gráfica da UFRGS, pp. 13–71.

Hartmann, L.A., Duarte, L.C., Massonne, H.-J., Michelin, C., Rosenstengel, L.M., Bergmann, M., Theye, T., Pertille, J., Arena, K.R., Duarte, S.K., Pinto, V.M., Barboza, E.G., Rosa, M.L.C.C., Wildner, W., 2012. Sequential opening and filling of cavities forming vesicles, amygdales and giant amethyst geodes in lavas from the southern Paraná volcanic province, Brazil and Uruguay. International Geology Review 54, 1–14.

Hurst, A., Scott, A., Vigorito, M., 2011. Physical characteristics of sand injectites. Earth-Science Reviews 106, 215–246.

Huuse, M., Shoulders, S.J., Netoff, D.I., Cartwright, J., 2005. Giant sandstone pipes record basin-scale liquefaction of buried dune sands in the Middle Jurassic of SE Utah. Terra Nova 17, 80–85.

Huuse, M., Jackson, C.A.L., Rensbergen, P.V., Davies, R.J., Flemings, P.B., Dixon, R.J., 2010. Subsurface sediment remobilization and fluid flow in sedimentary basins: an overview. Basin Research 22, 342–360.

Jacques, P.D., Machado, R., Nummer, A.R., 2010. Lineamentos estruturais na borda leste da Bacia do Paraná em Santa Catarina: análise multiescala com base em imagens LANDSAT e SRTM. Pesquisas em Geociências-Universidade Federal do Rio Grande do Sul 37, 117–131.

Janasi, V.A., Freitas, V.A., Heaman, L.H., 2011. The onset of flood volcanism, Northern Paraná Basin, Brazil: a precise U–Pb baddeleyite/zircon age for a Chapecó-type dacite. Earth and Planetary Science Letters 302, 147–153.

Jébrak, M., 1997. Hydrothermal breccias in vein-type ore deposits: a review of mechanisms, morphology and size distribution. Ore Geology Reviews 12, 111–134.

Johari, A., Taib, M.R., 2007. Effect of sand sizes on the fluidization behavior in circular and rectangular columns. Journal of Chemical and Natural Resources Engineering-UniversitiTeknologi Malaysia 2, 14–21.

Levi, T., Weinberger, R., Eyal, Y., 2011. A coupled fluid-fracture approach to propagation of clastic dikes during earthquakes. Tectonophysics 498, 35–44.

Machado, F.B., Nardy, A.J.R., Rocha Jr., E.R.V., Marques, L.S., Oliveira, M.A.F., 2009. Geologia e litogeoquímica da Formação Serra Geral nos estados de Mato Grosso e Mato Grosso do Sul. Geociências-Universidade Estadual Paulista 28, 523–540.

Mazurek, J., 2004. Genetic controls on basalt alteration within the eastern Snake River plain aquifer, Idaho. Masters of Science thesis, Department of Geosciences, Idaho State University.

Morteani, G., Kostitsyn, Y., Preinfalk, C., Gilg, H.A., 2010. The genesis of the amethyst geodes at Artigas (Uruguay) and the paleohydrology of the Guaraní aquifer: structural, geochemical, oxygen, carbon, strontium isotope and fluid inclusion study. International Journal of Earth Sciences 99, 927–947.

Neuhoff, P.S., Rogers, K.L., Stannius, L.S., Bird, D.K., Pedersen, A.K., 2006. Regional very low-grade metamorphism of basaltic lavas, Disko–Nuussuaq region, West Greenland. Lithos 92, 33–54.

Peate, D.W., Hawkesworth, C.J., Mantovani, M.S.M., 1992. Chemical stratigraphy of Paraná lavas (South America): classification of magma types and their spatial distribution. Bulletin of Volcanology 55, 119–139.

Perinotto, J.A.J., Etchebehere, M.L.C., Simões, L.S.A., Zanardo, A., 2008. Diques clásticos na Formação Corumbataí no nordeste da Bacia do Paraná, SP: Análise sistemática e significações estratigráficas, sedimentológicas e tectônicas. Geociências– Universidade Estadual Paulista 27, 469–491.

Petry, K., Jerram, D.A., Almeida, D.P.M., Zerfass, H., 2007. Volcanic-sedimentary features in the Serra Geral Fm., Paraná Basin, southern Brazil: examples of dynamic lava–sediment interactions in an arid setting. Journal of Volcanology and Geothermal Research 159, 313–325.

Pinto, V.M., Hartmann, L.A., Santos, J.O.S., McNaughton, N.J., Wildner, W., 2011a. Zircon U–Pb geochronology from the Paraná bimodal volcanic province support a brief eruptive cycle at 135 Ma. Chemical Geology 281, 93–102.

Pinto, V.M., Hartmann, L.A., 2011. Flow-by-flow chemical stratigraphy and evolution of thirteen Serra Geral Group basalt flows from Vista Alegre, southernmost Brazil. Anais da Academia Brasileira de Ciências 83, 425–440.

Pinto, V.M., Hartmann, L.A., Wildner, W., 2011b. Epigenetic hydrothermal origin of native copper and supergene enrichment in the Vista Alegre district, Paraná basaltic province, southernmost Brazil. International Geology Review 43, 1163–1179.

Salaün, A., Villemant, B., Gérard, G., Komorowski, J.-C., Michel, A., 2011. Hydrothermal alteration in andesitic volcanoes: trace element redistribution in active and ancient hydrothermal systems of Guadeloupe (Lesser Antilles). Journal of Geochemical Exploration 111, 59–83.

Scherer, C.M.S., 2000. Eolian dunes of the Botucatu Formation (Cretaceous) in southernmost Brazil: morphology and origin. Sedimentary Geology 137, 63–84.

Schwab, A.M., Jameson, E.W., Townsley, A., 2011. Development of a sand injection complex: Volund Field, Offshore Norway. AAPG Annual Conference and Exhibition. Houston, Texas, abstract. 1 pp.

Tamas, C.G., Milési, J.-P., 2003. Hydrothermal breccia pipe structures – general features and genetic criteria – II. Phreatic breccias. StudiaUniversitatis, Babes-Bolyai. Geologia, XLVIII, pp. 55–66.

Vétel, W., Cartwright, J., 2010. Emplacement mechanics of sandstone intrusions: insights from the Panoche Giant Injection Complex, California. Basin Research 22, 783–807.

Waichel, B.L., Lima, E.F., Lubachesky, R., Sommer, C.A., 2007. Peperite formed by lava flows over sediments: an example from the central Paraná Continental Flood Basalts, Brazil. Journal of Volcanology and Geothermal Research 159, 343–354.

Walker, R.J., Holdsworth, R.E., Imber, J., Ellis, D., 2011. The development of cavities and clastic infills along fault-related fractures in Tertiary basalts on the NE Atlantic margin. Journal of Structural Geology 33, 92–106.

Zalán, P.V., Wolff, S., Astolfii, M.A.M., Vieira, I.S., Conceição, J.C.J., Appi, V.T., Neto, E.V.S., Cerqueira, J.R., Marques, A., 1991. The Paraná basin, Brazil. In: Leighton, M.W., Kolata, D.R., Oltz, D.F., Eidel, J.J. (Eds.), Interior Cratonic Basins: American Association of Petroleum Geologists Memoir, 51, pp. 681–708.